coatings

MDPI

Communication

Oxidation Behavior of Lightweight $Al_{0.2}CrNbTiV$ High Entropy Alloy Coating Deposited by High-Speed Laser Cladding

Tianhui Chen [1], Zhijiang Bi [1], Ji Zhou [1], Ruohui Shuai [1], Zhihai Cai [2], Liyan Lou [1,*], Haidou Wang [2] and Zhiguo Xing [2]

[1] National-Local Joint Engineering Laboratory of Intelligent Manufacturing Oriented Automobile Die & Mould, Tianjin University of Technology and Education, Tianjin 300222, China; 18094494007@163.com (T.C.); 15531955076@163.com (Z.B.); m15522392405_1@163.com (J.Z.); 15770529201@163.com (R.S.)

[2] National Engineering Research Center for Remanufacturing, Army Academy of Armored Forces, Beijing 100072, China; caizhihai2052@163.com (Z.C.); wanghaidou@aliyun.com (H.W.); xingzg2011@163.com (Z.X.)

* Correspondence: louly88@126.com

Abstract: High-temperature oxidation resistance is the major influence on the high-temperature service stability of refractory high entropy alloys. The oxidation behavior of lightweight $Al_{0.2}CrNbTiV$ refractory high entropy alloy coatings with different dilution ratios at 650 °C and 800 °C deposited by high-speed laser cladding was analyzed in this paper. The oxidation kinetic was analyzed, the oxidation resistance mechanism of the $Al_{0.2}CrNbTiV$ coating was clarified with the analysis of the formation and evolution of the oxidation layer, and the effect of the dilution rate on high-temperature performances was revealed. The results showed that the oxide layer was mainly composed of rutile oxides (Ti, Cr, Nb)O_2 after isothermal oxidation at 650 °C and 800 °C for 50 h. The $Al_{0.2}CrNbTiV$ coating in low dilution exhibited better oxidation performance at 650 °C, due to the dense oxide layer formed with the synergistic growth of fine $AlVO_3$ particles and (Ti, Cr, Nb)O_2, and higher percentage of Cr, Nb in (Ti, Cr, Nb)O_2 strengthened the lattice distortion effect to inhibit the penetration of oxygen. The oxide layer formed at 800 °C for the $Al_{0.2}CrNbTiV$ coating was relatively loose, but the oxidation performance of the coating in high dilution improved due to the precipitation of Cr_2Nb-type Laves phases along grain boundaries, which inhibits the diffusion of oxygen.

Keywords: high-speed laser cladding; high-entropy alloys; oxidation behavior; coating

Citation: Chen, T.; Bi, Z.; Zhou, J.; Shuai, R.; Cai, Z.; Lou, L.; Wang, H.; Xing, Z. Oxidation Behavior of Lightweight $Al_{0.2}CrNbTiV$ High Entropy Alloy Coating Deposited by High-Speed Laser Cladding. *Coatings* **2024**, *14*, 1104. https://doi.org/10.3390/coatings14091104

Academic Editor: Angela De Bonis

Received: 18 July 2024
Revised: 14 August 2024
Accepted: 16 August 2024
Published: 1 September 2024

1. Introduction

The refractory high entropy alloys (RHEAs) proposed in 2010 could have extremely high temperature strength due to the addition of refractory elements with high melting points such as W, Hf, Ta, Zr, Nb, etc. [1]. Thus, RHEAs are expected to become the next generation of high-temperature materials following nickel-based alloys. However, the application of RHEAs still faces the problem of high density, poor room temperature toughness and insufficient resistance to high temperature oxidation. The density and the ductility of RHEAs could be improved through control of the chemical composition. For example, the lightweight $Al_{0.5}CrNbTi_2V_{0.5}$ RHEA had a yield strength of 1240 MPa, and no fracture occurred after 50% compression [2]. We also proposed a lightweight RHEA-$Al_{0.2}CrNbTiV$ [3], which has a low density of 6.38 g/cm^3 and shows a combination of strength and ductility at room temperature, with a yield strength of 1570 MPa and deformation in compression $\varepsilon > 50\%$.

Nevertheless, insufficient oxidation resistance remains the main constraint for the high-temperature application of RHEAs. The main reason is the poor antioxidant property of the refractory elements, such as W and Mo. A pesting-like phenomenon, a kind of accelerated formation of oxides with unfavorable volumetric expansion, is even prone to occur in RHEAs, such as $Hf_{0.5}Nb_{0.5}Ta_{0.5}Ti_{1.5}Zr$ [4] and TiZrNbHfTa [5], similar to conventional

refractory elements and alloys. The addition of elements such as Al, Cr, Si, etc., has been proved to enhance the high-temperature oxidation resistance of RHEAs and suppress the "pest" phenomenon. For the TiZrNbHfTa alloy [6], a large amount of oxide powder is formed with a sharp weight gain after oxidation at 700–900 °C for 10 h, indicating a poor ability to resist oxygen corrosion. With the addition of Al, a relatively stable composite oxide layer can be formed on the surface of AlTiZrNbHfTa, but its oxidation weight gain was still higher than nickel-based alloys after being oxidized at 1100 °C for 1 h. In the long-term oxidation performance research on lightweight AlNbTiZr conducted by Jayaraj et al. [7], a composite oxide film mainly composed of $AlNbO_4$ and Ti_2ZrO_6 was formed after oxidation for 50 h at 600, 800, and 1000 °C, which was relatively dense and could prevent oxidation to some extent. Despite the addition of elements, continuous and dense single oxide films such as Al_2O_3, Cr_2O_3, or SiO_2 were still difficult to form for RHEAs, with composite oxide films appearing instead [5,8,9]. However, recent research results indicate that composite oxide films such as $CrNbO_4$ and $CrTaO_4$ have relatively low growth rates, and could provide good protective properties during high-temperature oxidation [10], giving rise to new ideas for improving the high-temperature oxidation resistance of RHEAs.

High-speed laser cladding technology (HSLC) can efficiently deposit thin, dense, and metallurgically bonded coatings. In our previous work, lightweight $Al_{0.2}$CrNbTiV RHEA coatings with a BCC solid solution structure were prepared by HSLC, which had thicknesses of 150–450 μm, for dilutions between 2.4% and 33.6%. Thus, the hardness and resistance to plastic deformation of the titanium alloy substrate was enhanced. In this paper, the oxidation behavior of the high-speed laser cladded $Al_{0.2}$CrNbTiV RHEA coating is further analyzed, clarifying the oxidation behaviors of the coatings at different temperatures, and the mechanism of the dilution ratio on the oxidation process.

2. Materials and Experiments

The substrate was a commercial TC4 (Ti-6Al-4V) titanium alloy rod with a diameter of 30 mm. The cladding material was atomized $Al_{0.2}$CrNbTiV RHEAs spherical powder, with a particle size of 50–150 μm, and composition as shown in Table 1.

Table 1. Chemical composition of Al0.2CrNbTiV RHEA powder (at.%).

Element	Al	Cr	Nb	Ti	V
Nominal composition	4.76	23.81	23.81	23.81	23.81
Test composition	5.41	23.41	23.62	24.08	23.47

A 2.5 kW semiconductor laser (RFL A2500D, Ruike Fiber Laser Technology Ltd., Wuhan, China) with a fiber coupled output was used as the heat source. A Gaussian shaped laser beam profile and laser spot of Φ2.5 mm and a self-designed co-axial powder feeding nozzle were chosen during the laser cladding process. The experiment was carried out inside a protective gas box with continuously injected argon (99.99%, flow rate 0.5 L/min) to prevent the oxidation of the coating. The processing parameters were chosen to control the dilution of the coating based on our previous work. The low-dilution (3.1%) coating with finer grains was recorded as LC1.5, and the high-dilution coating (31.9%), which exhibited stronger epitaxial growth tendency and coarser grains was recorded as LC2.0. The processing parameters of the coating are shown in Table 2. The microstructure of the coatings and preparation details can be found in previous research.

The high-temperature isothermal oxidation tests were conducted in a muffle furnace under ambient conditions for 50 h. Considering the lower melting point of vanadium oxides of ~680 °C and the α trans temperature of TC4 alloy of 880 °C [11], moderate oxidation temperatures of 650 °C and 800 °C were chosen in this research. Samples were cut from the as-prepared substrates with coatings using the spark-erosion wire cutting method, placed in the furnace, heated up and cooled to the target temperatures at a rate of 5 °C/min. After removal from the furnace, the mass gain of both coated and uncoated samples was

measured using an electronic weight balance machine with an accuracy of ±0.1 mg, and three parallel specimens were measured each time to eliminate measurement error.

Table 2. Laser cladding process parameters of HSLC.

Coating	Laser Power (kW)	Working Distance (mm)	Gas Flow Rate (L/min)	Deposition Speed (mm/s)	Overlapping Ratio (%)	Powder Flow Rate (g/min)
LC1.5	1.5	15	6	157	70	23.22
LC2.0	2	15	6	157	70	14.16

The phase structure and constituent phases of the oxidized coating were determined with X-ray diffraction (XRD, Bruker D8 ADVANCE A25, Bruker, Germany), performed with Cu-Ka radiation at 40 kV, and scanning speed of 0.02°/s. The microstructure and elemental analysis were conducted with a Hitachi S-3400 Scanning Electron Microscope (SEM, Hitachi, S3400, Japan manufacturer, Tokyo, Japan) equipped with Energy-Dispersive Spectrometer (EDS).

3. Results

As the oxidation progressed, the coated alloys started to gain weight with no spallation or pesting-like phenomenon exhibited. The weight gain of the coatings LC1.5 and LC2.0 after oxidation at 650 °C was significantly lower than at 800 °C, indicating better oxidation resistance at 650 °C (Figure 1).

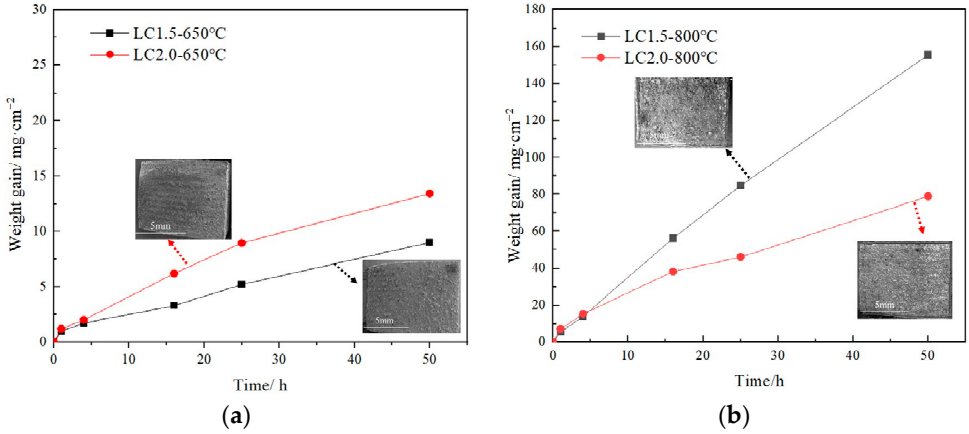

Figure 1. Oxidation kinetics curves of $Al_{0.2}CrNbTiV$ coating: (**a**) Oxidation at 650 °C; (**b**) Oxidation at 800 °C.

When oxidizing isothermally at 650 °C, coating LC1.5 had the lowest mass gain, with the oxidation kinetics following $(\Delta m)^{1.86} = 1.23 \cdot t$. The nearly parabolic oxidation rate exponent meant that a protective oxide layer (OL) could be formed (Figure 1a), which inhibited the diffusion of oxygen into the coating, and reduced the rate of oxidation.

When oxidizing at 800 °C, the coatings with different dilution rates showed a linear kinetic with a sharp increase in mass (Figure 1b), which meant that a loose non-protective oxide film was formed, which could not block the diffusion of oxygen. It is interesting to observe that LC1.5 possessed both the lowest and highest mass gain at different temperatures.

The oxides formed at different temperatures were dominated by rutile oxides, as seen in Figure 2. Besides TiO_2, the formation of rutile oxides $Ti_{0.2}Cr_{0.4}Nb_{0.4}O_2$, $Ti_{0.4}Cr_{0.3}Nb_{0.3}O_2$, etc., was also detected, indicating that during the oxidation process, different elements in the multi-major alloys reacted synergistically, and the alloying elements did not appear in the form of a single metal oxide. Simultaneously, $AlVO_3$ was formed at 650 °C. However, when oxidized at 800 °C, rutile oxides were the sole oxidation product.

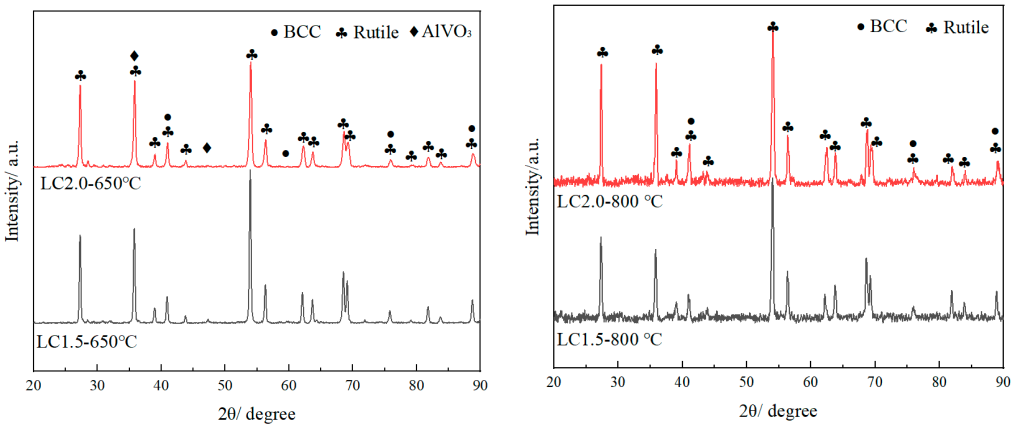

Figure 2. XRD patterns of $Al_{0.2}CrNbTiV$ coatings after oxidation: (**a**) Oxidation at 650 °C for 50 h; (**b**) Oxidation at 800 °C for 50 h.

After isothermal oxidation at 650 °C for 50 h, the OL of coatings LC1.5 and LC2.0 appeared adherent with no visible pores and cracks formed, which could play a role in hindering the intrusion of oxygen, in thicknesses were 11.5 μm and 21.5 μm, respectively, as shown in Figure 3a,b, with corresponding EDS analysis in Table 3. Both of the OLs were composed of rutile oxides, enriched in Ti-, Cr-, Nb-, with small amounts of Al and V dissolved, denoted as (Ti, Cr, Nb)O_2.

Table 3. Elemental distribution (at.%) of $Al_{0.2}CrNbTiV$ coatings after oxidation.

Coating	Region	O	Al	Ti	V	Cr	Nb
LC1.5-650 °C	Point A	63.54	16.82	0.45	15.50	3.67	0.02
	Oxide layer	63.58	1.68	9.31	6.3	9.68	9.45
LC2.0-650 °C	Point B	65.35	15.35	0.76	16.52	1.94	0.09
	Point C	59.75	13.24	7.26	13.83	3.63	2.30
	Point D	33.75	6.53	45.58	5.13	3.56	5.45
	Oxide layer	69.40	2.33	15.93	3.94	4.06	4.34
LC1.5-800 °C	Point E	44.94	5.46	17.44	10.38	9.54	12.24
	Point F	25.89	2.51	13.23	19.04	21.99	17.35
	Oxide layer	68.80	1.93	8.98	2.78	8.73	8.78
LC2.0-800 °C	Point G	34.39	4.65	49.90	3.64	2.54	4.87
	Point H	9.40	0.33	19.10	17.20	39.41	14.56
	Oxide layer	70.57	1.09	17.83	2.23	3.71	4.57

For coating LC1.5, (Ti, Cr, Nb)O_2 exhibited in granular particles. Particles were formed as needle-type for coating LC2.0. The reason for this difference could be the substantially increased Ti content of coating LC2.0 due to the high dilution; and densification of the OL of the coating LC2.0 would also be affected as slender oxide enabled a faster growth rate [12,13]. Dark-gray $AlVO_3$ particles in different sizes (point A and white arrows in Figure 3a) were distributed inside or on the surface of the OL. A large amount of fine $AlVO_3$ particles coexisted with (Ti, Cr, Nb)O_2 and embedded in the OL, which meant that the (Ti, Cr, Nb)O_2 and $AlVO_3$ could grow synergistically, making the OL of coating LC1.5 denser. At the same time, coarse-shaped $AlVO_3$ particles (point B, Figure 3b) were dispersed upon the OL or segregated to form blocky features (point C, Figure 3b) for coating LC2.0.

Internal oxidation refers to the phenomenon that oxygen in the environment passes through the OL, dissolves in the alloy, reacts with one or more alloying elements, generates internal oxide precipitates in the sublayer, and disperses in the metal phase to form an internal oxidized zone. This has become a common phenomenon for the high temperature

oxidation of RHEAs. For coating LC1.5, the microstructure of the coated zone adjacent to the OL still kept a dendritic structure in the deposited state (blue box in Figure 3a), and only an oxygen enriched area was formed (area above the white dashed line, Figure 3a). For coating LC2.0, significant internal oxidation occurred (blue box in Figure 3b), as needle-like structures in dark gray were formed (point D, Figure 3b) with the preferential oxidation of Ti and Al. Meanwhile, the histomorphology of the internal oxidized zone of coating LC2.0 indicated that oxygen penetrated the OL into the coating, diffused and oxidized along the grain boundaries, that is, volume diffusion occurred. Oxygen continued to diffuse along the inter-dendritic network and infiltrated into the dendrites, gradually oxidizing the dendrites of the coating. Therefore, coating LC1.5 in low dilution was more effective in limiting the oxygen ingress into the coating with the formation of the relatively denser OL.

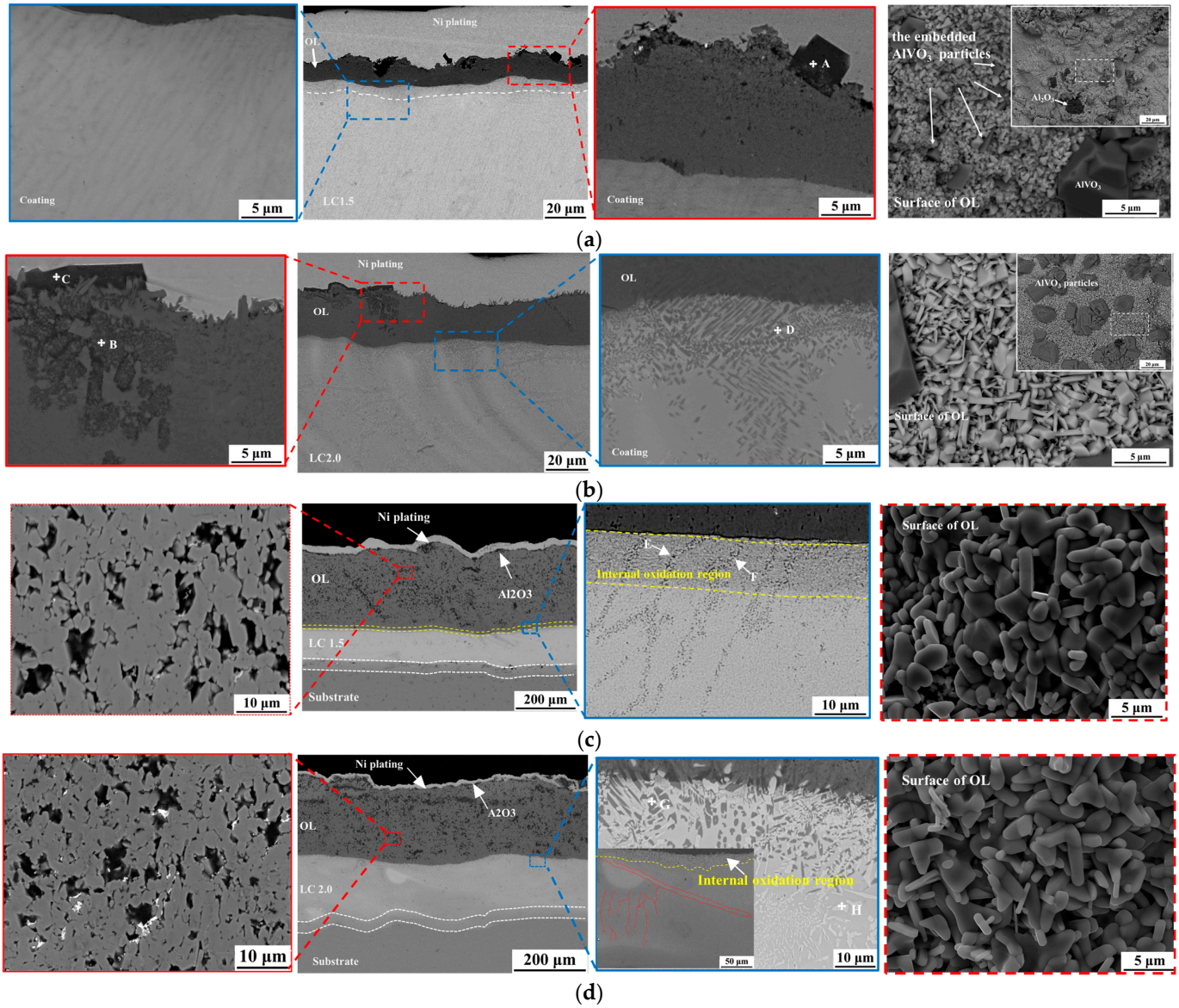

Figure 3. Microstructure of coating after oxidation: (**a**) LC1.5 at 650 °C; (**b**) LC2.0 at 650 °C; (**c**) LC1.5 at 800 °C; (**d**) LC2.0 at 800 °C.

After oxidation at 800 °C for 50 h, the OLs of both coatings LC1.5 and LC2.0 became relatively loose with visible pores formed, and the thickness of the OL was up to 262 μm and 186 μm for coatings LC1.5 and LC2.0, respectively. Both the OLs were composed of rod-like rutile oxides (Figure 3c,d), consistent with the XRD results. Fine Al_2O_3 particles

could also be found, but no protective effect could be given. The decreased concentration of V element and low melting point of V_2O_5 (~680 °C) indicated the volatilization of V-oxides during oxidation. The vacancies left accelerate the diffusion of oxygen and the formation of the loosened OL.

Severe internal oxidation occurred after exposure at 800 °C for both of the coatings. For coating LC1.5, oxygen segregated in the internal oxidation region (yellow line region in Figure 3c), with intensely distributed Ti-, Al- enriched dark-gray oxides (point E, Figure 3c) and a white phase enriched in Cr and Nb, V with lower oxygen (point F, Figure 3c). Oxygen diffused rapidly along the grain boundary towards the depth of the coating below this region. At the same time, cracks parallel to the OL were also formed at the OL/coating interface due to the thermophysical matching problem between them, which further reduced the antioxidant performance. For coating LC2.0, a large quantity of Ti and Al enriched leaf-like oxides was precipitated (point G, Figure 3d) in the internal oxidation region (yellow line area in Figure 3d). The grain boundary diffusion of oxygen was not observed, but Cr enriched white phase (point H, Figure 3d) precipitated along the grain boundaries below and at the overlap "fusion line" (red lines in Figure 3d). EDS analysis and the previous research indicated that the precipitated Cr enriched white phase was Cr_2Nb-type Laves phase (Nb, Ti) $(Cr, Al, V)_2$ with a small amount of oxygen dissolved.

4. Discussion

Thermodynamic stability and kinetic growth laws determine the microstructural evolution of the oxide layer and determine its antioxidant properties [14]. The standard Gibbs free energies of the thermodynamically stable oxides of $Al_{0.2}CrNbTiV$ are shown in Figure 4. Among them, $AlVO_3$, a spinel phase with a corundum structure, can be thermodynamically stable at atmospheric pressure of 1300 °C, and can be assumed to be formed through the chemical reaction of Al_2O_3 and V_2O_3 in Equation (1) [15,16], and its standard free can be calculated by Equation (2):

$$\frac{1}{2}Al_2O_3(s) + \frac{1}{2}V_2O_3(s) = AlVO_3(s) \quad (1)$$

$$\Delta G^0_{AlVO_3} = \frac{1}{2}\Delta G^0_{Al_2O_3} + \frac{1}{2}\Delta G^0_{V_2O_3} \quad (2)$$

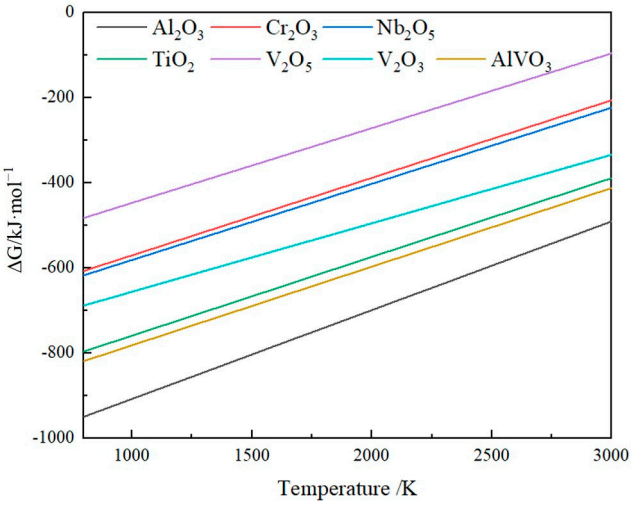

Figure 4. Standard Gibbs free energy for different oxides.

The graphs for calculated Gibbs free energies shown in Figure 4 indicate that Al_2O_3 and $AlVO_3$ have the lowest value among all of the thermally stable oxides, followed by TiO_2. However, the Ti content in the coating is much higher than Al, giving the formation of TiO_2 an advantage. At the same time, TiO_2 has a high solubility for other elements; Cr,

Nb, and V atoms can occupy Ti sites in a rutile lattice, making large amounts of (Ti, Cr, Nb)O_2. Non-stoichiometric rutile oxides can be formed quickly and become dominant in the OL. Since multiple elements reacted and dissolved synergistically, single-element oxides failed to form except for a small amount of Al_2O_3 or $AlVO_3$, and (Ti, Cr, Nb)O_2 rutile-type oxides dominated the oxide layers at different temperatures.

It should be noted that both the oxidation temperature and the coating composition affected the morphology of (Ti, Cr, Nb)O_2, which could exhibit in particles of a needle or rod type. The (Ti, Cr, Nb)O_2 formed at 800 °C for coating LC1.5 and LC2.0 was of a rod type, much coarser than when it formed at 650 °C reducing the densification of the OL significantly. For coating LC2.0, with a higher percentage of Ti in high dilution, 3~4 times higher than other elements, (Ti, Cr, Nb)O_2 grew in a needle type with a faster growth rate, different from the granular particles for coating LC1.5 when oxidizing at 650 °C. The reason was that the substitution of Nb^{5+} for Ti^{4+} in TiO_2 could reduce the oxygen vacancy concentration and inhibit the growth of oxide, and the substitution of Cr for Ti could decrease the lattice parameter, making the migration of the oxygen atoms more difficult. At the same time, Al atoms could occupy the interstitial position in the rutile lattice, inhibiting oxygen diffusion with reduced anion vacancy concentration. The XRD pattern in Figure 2a also shows that the lattice parameters of the rutile were a = 4.619 Å and c = 2.987 Å for coating LC1.5 and a = 4.618 Å and c = 2.980 Å for coating LC2.0; both were larger than the TiO_2 standard card (ICDD #01-073-1782), with a = 4.593 Å and c = 2.959 Å, indicating a strengthened lattice distortion effect in the (Ti, Cr, Nb)O_2. Therefore, with the increase of the content of Al, Cr, Nb, and V in coating LC1.5, the disorder of the "rutile solid solution" increases, i.e., the entropy value increases, which decreases the oxygen diffusion process and reduces the oxidation rate.

At the same time, the results of previous work showed that coating LC1.5 had finer grain size, which meant a higher volume fraction of the grain boundaries; this could enhance the short-path diffusion of elements and accelerate the formation of the protective oxide layer. During isothermal oxidation at 650 °C, finer grains of coating LC1.5 accelerated the formation of the protective OL, the synergistic growth of fine $AlVO_3$ particles and (Ti, Cr, Nb)O_2 promoted the densification of the OL, and the rutile oxides with dissolved Al, Cr, Nb, and V enhanced the lattice distortion, the ingress of oxygen was prevented more effectively, thus coating LC1.5 exhibited better oxidation performance than coating LC2.0. The oxidation behavior at 650°of different coatings is shown schematically in Figure 5.

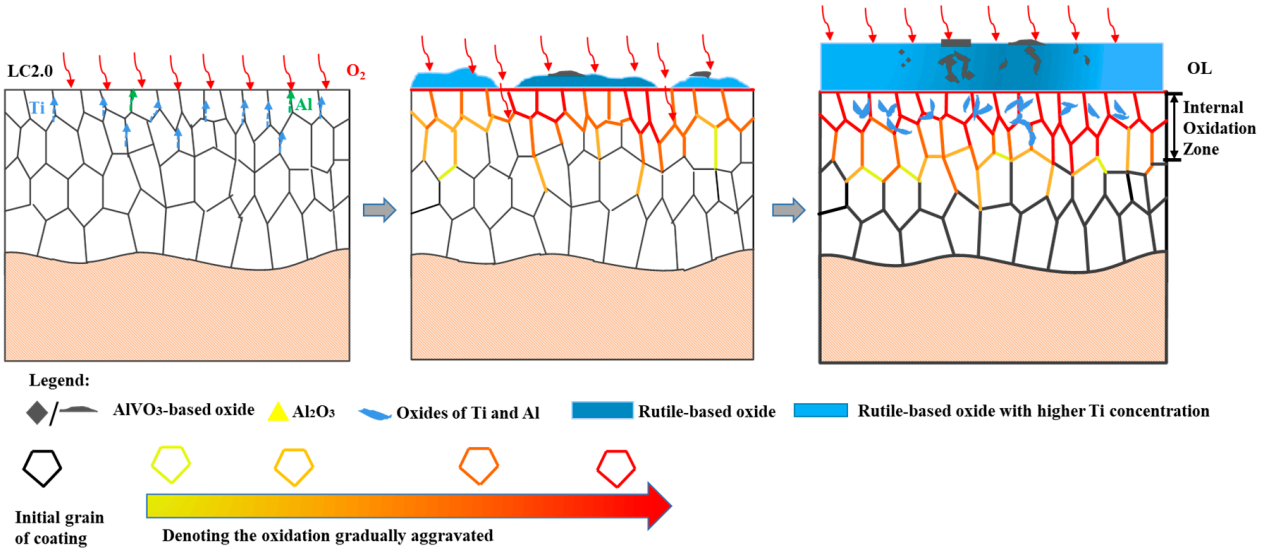

Figure 5. Schematic diagram of oxidation behavior of $Al_{0.2}$CrNbTiV coating at 650 °C.

Upon isothermal oxidation at 800 °C, a loose OL was formed by the accumulation of rod-like (Ti, Cr, Nb)O_2 for coatings LC1.5 and LC2.0. The oxidation process was con-

trolled by the external diffusion of metal elements. Furthermore, the formation of the non-protective OL was accelerated in coating LC1.5 due to its finer grains. Although both the coatings underwent severe internal oxidation with the precipitation of the Laves phase, for coating LC2.0, due to fewer nucleation sites under coarse columnar grains, the Laves phase preferentially precipitated along grain boundaries. The Laves phase precipitation along the grain boundary can play a role in reducing the oxygen diffusion channel and inhibiting the oxidation process, delaying the transition from internal oxidation to external oxide layer, such that the oxidation performance of coating LC2.0 at 800 °C improved. For coating LC1.5, the rapidly precipitated Laves phase could not hinder the diffusion of oxygen, and oxygen could diffuse rapidly along the grain boundaries (Figure 3c). Meanwhile, the internal stress caused by the precipitation of oxides along the grain boundaries further promoted the nucleation and growth of new oxides at the grain boundaries, weakening the oxidation performance of coating LC1.5.

High-temperature oxidation resistance has become the major obstacle for the high-temperature application of RHEAs, but research about the oxidation behavior of RHEAs is scarce compared with the transition group high entropy alloys. Similar to most RHEAs, in the present study, after oxidation at 650 °C and 800 °C, the composite OL was formed, dominated by rutile (Ti, Cr, Nb)O_2, instead of the continuous and dense single Al_2O_3 or Cr_2O_3 oxide film although Al and Cr existed in the Al-Cr-Nb-Ti-V alloy system. At 650 °C, due to the dense structure and the enhanced lattice distortion effect of (Ti, Cr, Nb)O_2, the OL still could prevent the interdiffusion of oxygen, and protect the titanium substrate from oxidation. At 800 °C, the mass gain of the $Al_{0.2}$CrNbTiV coating increased rapidly due to the porous OL. The slower oxidation rate of coating LC2.0 still reached 1.42 mg·cm^{-2}·h^{-1}. The mass gain of the $Al_{0.2}$CrNbTiV coating with different dilutions was higher than the traditional thermal protection materials MCrAlY. The HSLC deposited Cu-NiCoCrAlTaY coating had a mass gain of 5.93 mg·cm^{-2} under the same experiment conditions in our previous research [17]. The oxidation performance of $Al_{0.2}$CrNbTiV was worse than part of the RHEAs. As an example, for the AlTiVMoNb lightweight RHEA coating, the Al- containing oxide in the coating is the main oxidation product, followed by Ti oxide, and a small number of other oxides, giving a relatively lower mass gain of 4.94 mg·cm^{-2} [18]. In comparison, a NbTiZrV alloy, a kind of RHEA with high density, was completely oxidized after approximately 8 h of oxidation; the linear oxidation rate could be up to 1.42 mg·cm^{-2}·h^{-1} [11], much higher than the oxidation of $Al_{0.2}$CrNbTiV coating at 800 °C. Thus, the lightweight $Al_{0.2}$CrNbTiV coating has advantages of comprehensive mechanical properties and good oxidation resistance at moderate temperatures lower than 800 °C. In order to improve the high temperature performance, the chemical composition of the current Al-Cr-Nb-Ti-V alloy system could be optimized. The balance of the ductility and the oxidation performance should be considered, controlling the content of Al and Cr. The hindering effect of the Ti enriched rutile oxides on the formation of protective oxide scales such as Cr_2O_3, $AlCrO_4$, $AlNbO_4$, etc., may be investigated by adjusting Ti.

5. Conclusions

The oxide layer was mainly composed of (Ti, Cr, Nb)O_2 rutile oxides of the lightweight $Al_{0.2}$CrNbTiV RHEA coatings deposited by high-speed laser cladding after isothermal oxidation at 650 °C and 800 °C for 50 h.

The $Al_{0.2}$CrNbTiV coating in low dilution followed the rule $(\Delta m)^{1.86} = 1.23 \cdot t$ and exhibited good oxidation performance at 650 °C, due to the denser oxide layer and the (Ti, Cr, Nb)O_2 associated with stronger lattice distortion resulting from a higher percentage of Cr and Nb preventing the diffusion of oxygen.

The $Al_{0.2}$CrNbTiV coating followed linear kinetics at 800 °C with a loose oxide layer formed by the accumulation of rod-like (Ti, Cr, Nb)O_2. However, the Laves phase precipitated along grain boundaries inhibited the diffusion of oxygen, allowing the coating in high dilution to have better oxidation performance.

Author Contributions: Conceptualization, Z.C.; software, Z.B.; investigation, Z.B., J.Z. and R.S.; resources, L.L.; data curation, T.C.; writing—review and editing, T.C.; visualization, L.L., H.W. and Z.X. All authors have read and agreed to the published version of the manuscript.

Funding: This research was funded by Tianjin Natural Science Foundation (22JCYBJC01650), 145 project, National Natural Science Foundation of China (52130509), National key research and development program of China (No. 2021YFB4001400) and Key research and development plan of Shaanxi Province (S2023-YF-LLRH-QCYK-0201).

Institutional Review Board Statement: Not applicable.

Informed Consent Statement: Not applicable.

Data Availability Statement: Dataset available on request from the authors.

Acknowledgments: Xi'an Advanced Functional Coating Technology International Science and Technology Cooperation Base.

Conflicts of Interest: The authors declare no conflict of interest.

References

1. Senkov, O.; Wilks, G.; Miracle, D.; Chuang, C.; Liaw, P. Refractory high-entropy alloys. *Intermetallics* **2010**, *18*, 1758–1765. [CrossRef]
2. Stepanov, N.; Yurchenko, N.Y.; Panina, E.; Tikhonovsky, M.; Zherebtsov, S. Precipitation-strengthened refractory $Al_{0.5}CrNbTi_2V_{0.5}$ high entropy alloy. *Mater. Lett.* **2017**, *188*, 162–164. [CrossRef]
3. Li-Yan, L.; Shu-nan, C.; Yi, L.; Gang, J.; Hai-Dong, C.; Yun-Jie, J.; Chang-Jiu, L.; Cheng-Xin, L. Microstructure and mechanical properties of lightweight AlxCrNbTiV (x = 0.2, 0.5, 0.8) refractory high entropy alloys. *Int. J. Refract. Met. Hard Mater.* **2022**, *104*, 105784. [CrossRef]
4. Sheikh, S.; Shafeie, S.; Hu, Q.; Ahlström, J.; Persson, C.; Veselý, J.; Zýka, J.; Klement, U.; Guo, S. Alloy design for intrinsically ductile refractory high-entropy alloys. *J. Appl. Phys.* **2016**, *120*, 164902. [CrossRef]
5. Sheikh, S.; Bijaksana, M.K.; Motallebzadeh, A.; Shafeie, S.; Lozinko, A.; Gan, L.; Tsao, T.-K.; Klement, U.; Canadinc, D.; Murakami, H. Accelerated oxidation in ductile refractory high-entropy alloys. *Intermetallics* **2018**, *97*, 58–66. [CrossRef]
6. Chang, C.H.; Titus, M.S.; Yeh, J.W. Oxidation behavior between 700 and 1300 °C of refractory TiZrNbHfTa high-entropy alloys containing aluminum. *Adv. Eng. Mater.* **2018**, *20*, 1700948. [CrossRef]
7. Jayaraj, J.; Thirathipviwat, P.; Han, J.; Gebert, A. Microstructure, mechanical and thermal oxidation behavior of AlNbTiZr high entropy alloy. *Intermetallics* **2018**, *100*, 9–19. [CrossRef]
8. Lo, K.-C.; Yeh, A.-C.; Murakami, H. Microstructural investigation of oxidized complex refractory high entropy alloys. *Mater. Trans.* **2018**, *59*, 556–562. [CrossRef]
9. Liu, C.; Wang, H.; Zhang, S.; Tang, H.; Zhang, A. Microstructure and oxidation behavior of new refractory high entropy alloys. *J. Alloys Compd.* **2014**, *583*, 162–169. [CrossRef]
10. Butler, T.; Chaput, K.; Dietrich, J.; Senkov, O. High temperature oxidation behaviors of equimolar NbTiZrV and NbTiZrCr refractory complex concentrated alloys (RCCAs). *J. Alloys Compd.* **2017**, *729*, 1004–1019. [CrossRef]
11. Liang, Z.; Sun, Z.; Zhang, W.; Wu, S.; Chang, H. The effect of heat treatment on microstructure evolution and tensile properties of selective laser melted Ti_6Al_4V alloy. *J. Alloys Compd.* **2019**, *782*, 1041–1048. [CrossRef]
12. Sheikh, S.; Gan, L.; Ikeda, A.; Murakami, H.; Guo, S. Alloying effect on the oxidation behavior of a ductile $Al_{0.5}Cr_{0.25}Nb_{0.5}Ta_{0.5}Ti_{1.5}$ refractory high-entropy alloy. *Mater. Today Adv.* **2020**, *7*, 100104.
13. Lo, K.-C.; Murakami, H.; Yeh, J.-W.; Yeh, A.-C. Oxidation behaviour of a novel refractory high entropy alloy at elevated temperatures. *Intermetallics* **2020**, *119*, 106711. [CrossRef]
14. Zhang, Z.; Farahmand, P.; Kovacevic, R. Laser cladding of 420 stainless steel with molybdenum on mild steel A36 by a high power direct diode laser. *Mater. Des.* **2016**, *109*, 686–699. [CrossRef]
15. Landälv, L.; Carlström, C.-F.; Lu, J.; Primetzhofer, D.; Jõesaar, M.; Ahlgren, M.; Göthelid, E.; Alling, B.; Hultman, L.; Eklund, P. Phase composition and transformations in magnetron-sputtered $(Al,V)_2O_3$ coatings. *Thin Solid Film.* **2019**, *688*, 137369. [CrossRef]
16. Reid, A.; Sabine, T. AlVO3, a metal-deficient spinel. *J. Solid State Chem.* **1970**, *2*, 203–208. [CrossRef]
17. Li-Yan, L.; Yu, Z.; Yun-Jie, J.; Yan, L.; Hong-Fang, T.; Yu-Jun, C.; Cheng-Xin, L. High speed laser cladded Ti-Cu-NiCoCrAlTaY burn resistant coating and its oxidation behavior. *Surf. Coat. Technol.* **2020**, *392*, 125697. [CrossRef]
18. Chen, L.; Wang, Y.; Hao, X.; Zhang, X.; Liu, H. Lightweight refractory high entropy alloy coating by laser cladding on Ti–6Al–4V surface. *Vacuum* **2021**, *183*, 109823. [CrossRef]